J̶M RAPIDS

Highly singular slip length for longitudinal shear flow over a dense bubble mattress

Ehud Yariv†

Department of Mathematics, Technion – Israel Institute of Technology, Haifa 32000, Israel

Compound surfaces, consisting of periodic arrays of solid patches and free surfaces, exhibit hydrodynamic slipperiness which is quantified by their slip length. The limit of small solid fractions, where the slip length diverges, is of fundamental interest. This paper addresses longitudinal liquid flows over a periodic array of grooves which are partially invaded by the liquid. Assuming that the slats separating the grooves are infinitely thin, the solid fraction ϵ is set by the invasion depth. Inspired by the singular small-solid-fraction limit for non-invaded grooves (Schnitzer, *Phys. Rev. Fluids*, vol. 1, 2016, 052101R), we consider the idealised geometry of $90°$ protrusion angles, where an integral force balance in the limit $\epsilon \to 0$ implies a slip length that scales as ϵ^{-1}. The problem exhibits a nested structure, where the liquid domain is conceptually decomposed into four distinct regions: a unit-cell region on the scale of the period, where the wetted portion of the slat appears as a point singularity; two regions on the scale of the wetted slat, where the flow essentially varies in one dimension; and a transition region about the tip of the slat. Analysing these regions using matched asymptotic expansions and conformal mappings yields the ratio of slip length to semi-period as $2\epsilon^{-1} - (10/\pi) \ln 2 + \cdots$.

Key words: lubrication theory

1. Introduction

The advent of superhydrophobic surfaces, originally designed to facilitate conditions for non-wetting drops (Quéré 2005, 2008), has led to a surge in interest of liquid flows about microstructured surfaces consisting of solid patches and air bubbles (Rothstein 2010). The most common of these are periodic arrays of slats, with air bubbles trapped in the respective grooves (Ou & Rothstein 2005; Tsai *et al.* 2009), and doubly periodic pillar arrays, where air is trapped in the continuous region surrounding the pillars

† Email address for correspondence: yarivehud@gmail.com

(Joseph *et al.* 2006; Lee, Choi & Kim 2008). Owing to the dominance of capillarity at small scales, the liquid–air menisci are of uniform curvature. In particular, the cylindrical bubbles trapped in the groove-array surface possess the cross-sectional shape of a circular arc.

The slipperiness of a compound surface is characterised by the slip length (Bocquet & Barrat 2007), the fictitious distance below the surface at which an imposed shear profile extrapolates to zero. For the non-isotropic groove-array geometry, two canonical shear problems emanate: the 'longitudinal' one, where the shear is applied parallel the grooves; and the 'transverse' one, where it is applied perpendicular to them. The ratio of the slip length to the period depends upon the parameters quantifying the surface geometry, and in particular the solid fraction ϵ, representing (on a single period) the ratio of the wetted-solid area to the total area.

In modelling the canonical problem governing the slip length, it is common to neglect the viscosity of the trapped air. Since a free surface cannot support a shear force, the problem is ill-posed for $\epsilon = 0$ and is consequently singular for $\epsilon \ll 1$, implying a divergent slip length. A first illustration of that singularity was provided by Philip (1972) for both the longitudinal and transverse problems in the simplest case of flat menisci, where the corresponding slip-length formulae diverge as $\ln \epsilon$ (Lauga & Stone 2003). Given the pragmatic desire to maximise slip lengths (Choi & Kim 2006; Lee *et al.* 2008), there is a fundamental interest in understanding the small-solid-fraction singularity. A scaling analysis by Ybert *et al.* (2007) suggested an algebraic slip-length singularity, as $\epsilon^{-1/2}$, for the pillar-array configuration. For the groove-array configuration, no singularity was predicted; alluding to Philip (1972), Ybert *et al.* (2007) proposed a weak logarithmic singularity.

These scaling arguments were later tested against detailed analyses. While the $\epsilon^{-1/2}$ singularity was indeed confirmed for pillar arrays (Davis & Lauga 2010; Schnitzer & Yariv 2018), the predicted logarithmic singularity for groove arrays turns out to be incompatible with longitudinal slip-length calculations in the special case of 90° protrusion angles (Crowdy 2015). In a pioneering asymptotic analysis, Schnitzer (2016) showed that the singularity is in fact algebraic in that case, scaling as $\epsilon^{-1/2}$. Following that work, it was observed that 90° protrusion angles may lead to other peculiarities in longitudinal flows about groove arrays, such as an anomalous pressure-driven plug flow (Yariv & Schnitzer 2018).

The above investigations of groove-array geometries have been carried out assuming that the menisci are pinned at the edges of the slats. Under large pressures, however, the liquid may partially invade the grooves (Lee & Kim 2009; Lv *et al.* 2014). Thus, rather than being pinned, the contact lines of the liquid–air menisci are displaced a finite distance into the grooves. When modelling partially invaded configurations, one may conveniently take the slats to be infinitely thin (Crowdy 2021); the finite solid–liquid contact area on the sides of the slats, which vanishes in the 'conventional' non-invaded configuration, then effectively defines the solid fraction. For flat menisci, the longitudinal problem was solved in closed form by Crowdy (2021); consistently with the scaling arguments of Ybert *et al.* (2007), it exhibits a logarithmic singularity.

Crowdy (2021) also calculated the effect of small protrusion angles. As this results in a regular perturbation about the nominal flat-meniscus geometry, it also exhibits a logarithmic singularity. Presently, no analytic or numerical solution is known for finite protrusion angles. Inspired by the analysis of conventional surfaces (Schnitzer 2016), we here consider the partially invaded configuration in the extreme case of 90° protrusion angles, addressing the singular small-solid-fraction limit from the outset. Our goal is to illuminate the non-conventional singularity mechanism in that idealised configuration.
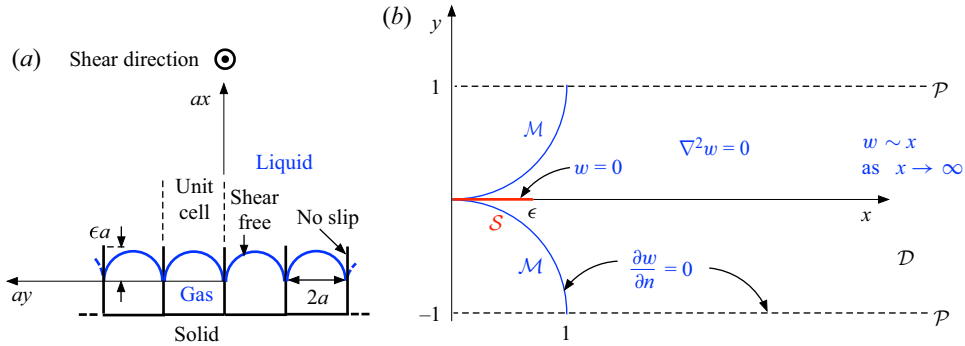
Figure 1. (*a*) Dimensional problem for a 90° protrusion angle bubble mattress. (*b*) Dimensionless unit-cell problem governing the longitudinal velocity.

2. Problem formulation

The microstructure considered herein consists of a periodic array (period $2a$) of slats, with air trapped in the enclosed grooves. The contact lines of the liquid–air menisci are displaced a finite distance ϵa ($\epsilon > 0$) into the grooves. Following earlier analyses (Crowdy 2021; Miyoshi *et al.* 2022), we assume that the slats are infinitely thin; then, ϵ represents the solid fraction of the microstructure. The curved menisci adopt a cross-sectional shape of a circular arc; we consider here the idealised scenario of a 90° protrusion angle, whereby a coincides with the bubble radius. The periodic geometry is portrayed in figure 1(*a*).

Following the canonical problem in the field (Davis & Lauga 2009), our interest is in the flow that is animated by an imposed shear (magnitude G) at large distances. We are concerned here only with the longitudinal problem which arises when the shear flow is pointing along the grooves. The flow is then unidirectional (Crowdy 2010), and the velocity is governed by a two-dimensional problem in the cross-sectional plane.

Normalising length variables by a, we employ Cartesian coordinates ($x_1 = x$, $x_2 = y$, x_3) with the xy plane perpendicular to the flow, the y axis passing through the contact lines (points in the cross-sectional plane), and the x axis passing through one of these lines, pointing into the liquid. Owing to periodicity, it suffices to consider a single 'unit cell', say, that bounded between $y = \pm 1$. The associated two-dimensional liquid domain, say, $\mathcal{D}$, is bounded by (i) the periodicity rays,

$$\mathcal{P}: \quad y = \pm 1, \quad x > 1; \tag{2.1}$$

(ii) the menisci,

$$\mathcal{M}: \quad y = \pm f(x), \quad 0 < x < 1, \tag{2.2}$$

where

$$f(x) = 1 - \sqrt{1 - x^2}; \tag{2.3}$$

and (iii) the solid slat,

$$\mathcal{S}: \quad 0 < x < \epsilon, \quad y = 0. \tag{2.4}$$

The fluid velocity, normalised by Ga, is $\hat{\boldsymbol{e}}_3 w$. The longitudinal component, $w(x, y; \epsilon)$, is governed by a unit-cell problem consisting of (i) Laplace's equation, $\nabla^2 w = 0$ in $\mathcal{D}$; (ii) the periodicity conditions, $\partial w / \partial y = 0$ on $\mathcal{P}$; (iii) the shear-free condition, $\partial w / \partial n = 0$
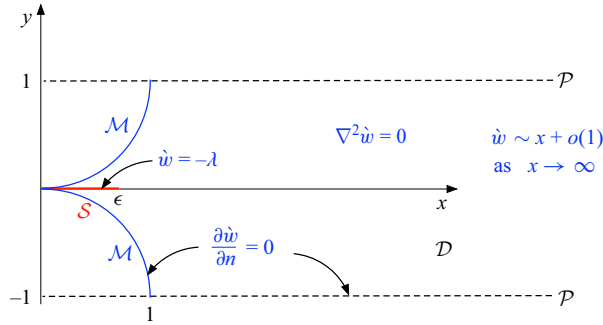
Figure 2. Unit-cell problem governing the excess velocity $\grave{w}$, as defined by (3.2).

on $\mathcal{M}$, wherein $\partial/\partial n$ is the normal derivative; (iv) the no-slip condition, $w = 0$ on $\mathcal{S}$; and (v) the imposed shear condition,

$$w \sim x \quad \text{as} \quad x \to \infty. \tag{2.5}$$

The unit-cell problem is described in figure 1(*b*).

The preceding problem determines the field w. In particular, it dictates the slip length λ in the asymptotic refinement of the imposed shear (2.5),

$$w = x + \lambda + o(1) \quad \text{as} \quad x \to \infty. \tag{2.6}$$

This constant, which depends only upon ϵ, is the quantity of interest.

3. Preliminaries

Assuming $\epsilon < 1$ and making use of the two-dimensional variant of Gauss's theorem and the homogeneous Neumann conditions on both $\mathcal{P}$ and $\mathcal{M}$, we find from Laplace's equation and the imposed shear (2.5) that

$$\int_{-f(x)}^{f(x)} \frac{\partial w}{\partial x} \, \mathrm{d}y = 2 \quad \text{for} \quad \epsilon < x < 1. \tag{3.1}$$

This 'flux balance' merely represents the transmission of shear forces in an inertia-free fluid (cf. Schnitzer 2016). Since (3.1) has been derived from the governing equations, it does not provide any independent information. Nonetheless, it is efficacious in the subsequent asymptotic analysis.

In what follows, it is convenient to employ the excess velocity

$$\grave{w} = w - \lambda. \tag{3.2}$$

Just like w, it satisfies Laplace's equation and the shear-free condition on $\mathcal{M}$. Rather than the no-slip condition, it satisfies the Dirichlet condition, $\grave{w} = -\lambda$ on $\mathcal{S}$. Moreover, while $\grave{w}$ also satisfies the imposed shear condition, expansion (2.6) implies that (2.5) is replaced by the more restrictive form,

$$\grave{w} = x + o(1) \quad \text{as} \quad x \to \infty. \tag{3.3}$$

The problem governing the excess velocity is delineated in figure 2. We note that the integral balance (3.1) still holds when w is replaced by $\grave{w}$.
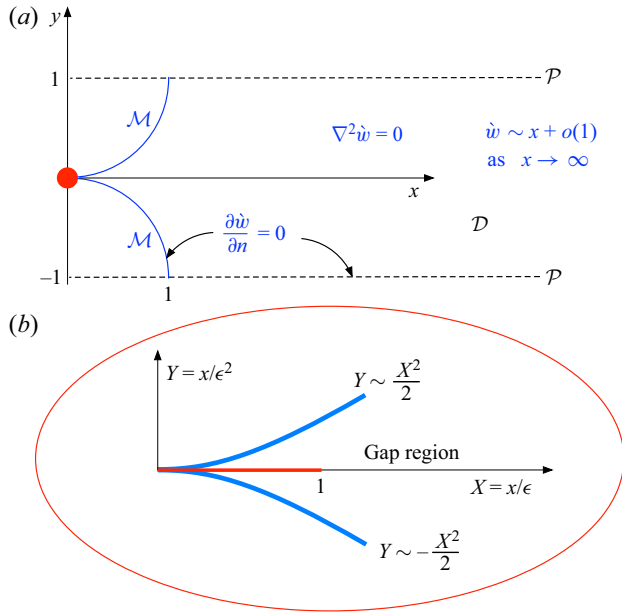
967 R3-4

Figure 3. Small-solid-fraction limit. (*a*) The period-scale leading-order problem is independent of λ, with a singularity at the origin. (*b*) Gap-scale geometry in the anisotropic stretching (4.1*a,b*).

4. Small-solid-fraction limit

When ϵ is asymptotically small, the line segment $\mathcal{S}$ shrinks to a point. The no-slip condition no longer applies; nonetheless, constraint (3.1) necessitates that $\dot{w}$ must become singular at the origin. The associated period-scale problem is described in figure 3. Since ϵ no longer appears in that problem, we expect $\dot{w}$ to be ord(1) on that scale.

The origin singularity is linked to the velocity field in the 'gap' region near the slat. In that region we find from (2.3) that $f(x) = x^2/2 + O(x^4)$. To perceive the slat, we focus upon $x = \text{ord}(\epsilon)$, whereby y is of order ϵ^2. From (3.1) we see that $\dot{w}$ is of order ϵ^{-1} in the gap region. The no-slip condition then gives $\lambda = \text{ord}(\epsilon^{-1})$.

To proceed beyond scaling, we employ the stretched coordinates (see figure 3),

$$x = \epsilon X, \quad y = \epsilon^2 Y, \tag{4.1a,b}$$

whereby $\mathcal{M}$ is given by $Y = \pm F(X; \epsilon)$, in which

$$F(X; \epsilon) = \frac{X^2}{2} + O(\epsilon^2). \tag{4.2}$$

Writing $\dot{w}(x, y; \epsilon) = W(X, Y; \epsilon)$, we find that the gap problem is governed by (i) the partial differential equation,

$$\frac{\partial^2 W}{\partial Y^2} + \epsilon^2 \frac{\partial^2 W}{\partial X^2} = 0; \tag{4.3}$$

(ii) the shear-free condition on $\mathcal{M}$,

$$\frac{\partial W}{\partial Y} = \pm\epsilon^2[X + O(\epsilon^2)]\frac{\partial W}{\partial X} \quad \text{at} \quad Y = \pm F(X; \epsilon); \tag{4.4}$$

(iii) the Dirichlet condition on $\mathcal{S}$,

$$W = -\lambda(\epsilon) \quad \text{at} \quad Y = 0 \quad \text{for} \quad 0 < X < 1; \tag{4.5}$$

(iv) conditions at $X \to \infty$, set by asymptotic matching with the period-scale solution; and
(v) the integral constraint (cf. (3.1)),

$$\int_{-F(X;\epsilon)}^{F(X;\epsilon)} \frac{\partial W}{\partial X} \, \mathrm{d}Y = 2\epsilon^{-1} \quad \text{for} \quad X > 1. \tag{4.6}$$

In contrast to the exact formulation, condition (4.6) now provides independent information.
    Given the identified scalings, we posit the asymptotic expansions,

$$W(X, Y; \epsilon) \sim \epsilon^{-1} W_{-1}(X, Y) + W_0(X, Y) + \cdots \tag{4.7}$$

and

$$\lambda(\epsilon) \sim \epsilon^{-1}\lambda_{-1} + \lambda_0 + \cdots . \tag{4.8}$$

5. Leading-order slip length

At ord(ϵ^{-1}) we find from (4.3) and (4.4) that W_{-1} is independent of Y, say, $W_{-1}(X)$. From
(4.5) we see that

$$W_{-1} \equiv -\lambda_{-1} \quad \text{for} \quad 0 < X < 1. \tag{5.1}$$

For $X > 1$ we get no information from (4.5). In this region, however, we may use (4.6),
which at ord(ϵ^{-1}) gives $\mathrm{d}W_{-1}/\mathrm{d}X = 2/X^2$ (see (4.2)). Integration yields

$$W_{-1} = -\frac{2}{X} + B_{-1} \quad \text{for} \quad X > 1. \tag{5.2}$$

Since the period-scale field $\mathring{w}$ is ord(1), asymptotic matching (Hinch 1991) necessitates
that $\lim_{X \to \infty} W_{-1} = 0$, which in turn implies $B_{-1} = 0$. We conclude that

$$W_{-1} = -\frac{2}{X} \quad \text{for} \quad X > 1. \tag{5.3}$$

    A continuous transition between (5.1) and (5.3) implies that

$$\lambda_{-1} = 2. \tag{5.4}$$

The derivative $\mathrm{d}W_{-1}/\mathrm{d}X$, however, is discontinuous at $X = 1$. We conclude the presence
of a 'corner layer' (Holmes 2012) about the slat tip which describes a smooth transition
between the 'left' gap region ($X < 1$), where (5.1) applies, and the 'right' gap region ($X >$
1), where (5.3) applies. Its resolution is required for the calculation of the ord(1) slip
length, which we consider next.

6. Calculation of the ord(1) slip

To proceed further, we need to address the leading-order period-scale flow. Since $\mathring{w} =$
ord(1), we write $\mathring{w}(x, y; \epsilon) \sim \mathring{w}_0(x, y) + \cdots$. The leading-order flow $\mathring{w}_0$ satisfies Laplace's
equation, the shear-free condition on $\mathcal{M}$ and the restricted far-field behaviour (3.3). In
addition, it satisfies the singularity condition,

$$\mathring{w}_0 \sim -\frac{2}{x} \quad \text{as} \quad (x, y) \to (0, 0), \tag{6.1}$$

obtained using asymptotic matching with the gap solution; see (5.3). Condition (6.1)
replaces the original no-slip condition; as it closes the leading-order period-scale problem,
the field $\mathring{w}_0$ may be considered as known.
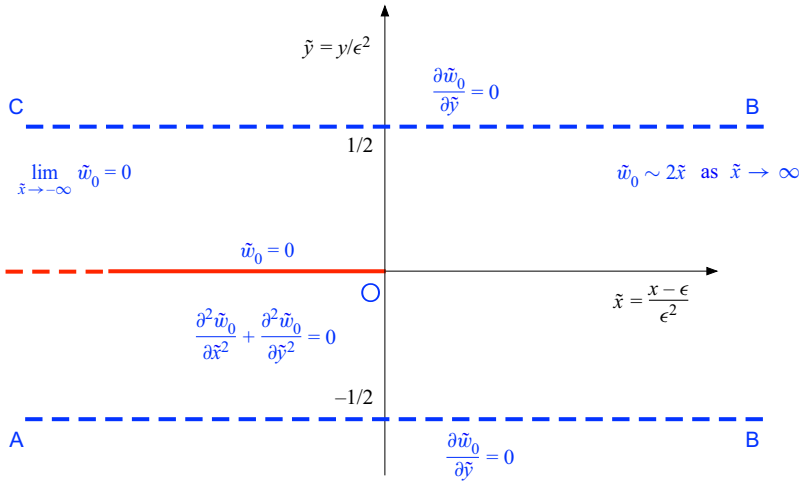
967 R3-6

Figure 4. Corner-layer geometry on $\mathrm{ord}(\epsilon^2)$ distances from the tip of the slat.

Consider now the gap region. From (4.3) and (4.4) at ord(1), we find that, just like W_{-1}, W_0 is a function of X alone, say, $W_0(X)$. From (4.5) we see that, in the left gap region (cf. (5.1)),

$$W_0 \equiv -\lambda_0 \quad \text{for} \quad 0 < X < 1. \tag{6.2}$$

To determine W_0 for $X > 1$ we observe using (4.2) that the integral (4.6) is trivial at ord(1). We conclude that W_0 is also uniform in the right gap region, say (cf. (5.2))

$$W_0 \equiv B_0 \quad \text{for} \quad X > 1. \tag{6.3}$$

Asymptotic matching yields the following refinement of (6.1):

$$\dot{w}_0 \sim -\frac{2}{x} + B_0 \quad \text{as} \quad (x, y) \to (0, 0). \tag{6.4}$$

Observing that the field $\bar{w}_0$ in Schnitzer (2016) coincides with the present $\dot{w}_0 - x$, we therefore obtain

$$B_0 = \lim_{(x,y)\to(0,0)} \left\{ \dot{w}_0 + \frac{2}{x} \right\} = \frac{12}{\pi} \ln 2. \tag{6.5}$$

7. Corner layer

At this stage we have two uniform solutions at the left and right gap regions, namely (6.2) and (6.3). Unlike the leading-order gap problem, however, continuity (which would naively imply that λ_0 is provided by $-B_0$) must be applied with care, accounting for a possible finite jump over the corner layer.

Since that layer must cover the entire cross-section of the gap, it is of linear extent $\mathrm{ord}(\epsilon^2)$. We thus write

$$x = \epsilon + \epsilon^2 \tilde{x}, \quad y = \epsilon^2 \tilde{y}. \tag{7.1a,b}$$

Note that $Y = \tilde{y}$ while $X = 1 + \epsilon \tilde{x}$. At leading order, the menisci $\mathcal{M}$ are given by $\tilde{y} = \pm 1/2$, while the slat is given by $\tilde{y} = 0$ with $\tilde{x} < 0$. The associated geometry is depicted in figure 4.
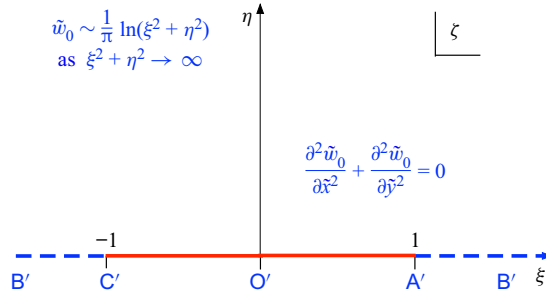
Figure 5. Auxiliary ζ plane, mapped to the corner region via the Schwarz–Christoffel transformation (8.6).

Here, we find it convenient to employ the original velocity field w, which is ord(1) in the corner region. Writing $w(x, y; \epsilon) = \tilde{w}(\tilde{x}, \tilde{y}; \epsilon)$, we expand it as $\tilde{w}_0(\tilde{x}, \tilde{y}) + \cdots$. The leading-order field $\tilde{w}_0$ is governed by (i) Laplace's equation in the Cartesian coordinates $(\tilde{x}, \tilde{y})$; (ii) the shear-free condition, $\partial \tilde{w}_0 / \partial \tilde{y} = 0$ at $\tilde{y} = \pm 1/2$; (iii) the no-slip condition, $\tilde{w}_0 = 0$ at $\tilde{y} = 0$ for $\tilde{x} < 0$; (iv) the decay condition, $\lim_{\tilde{x} \to -\infty} \tilde{w}_0 = 0$, which follows from asymptotic matching with the left gap region; and (v) the locally imposed shear,

$$\tilde{w}_0 \sim 2\tilde{x} \quad \text{as} \quad \tilde{x} \to \infty, \tag{7.2}$$

which follows from asymptotic matching with the right gap region; see (5.3). The preceding problem uniquely defines $\tilde{w}_0$.

Making use of asymptotic matching, we find that

$$\lambda_0 = \lim_{\tilde{x} \to \infty} (\tilde{w}_0 - 2\tilde{x}) - B_0. \tag{7.3}$$

Thus, evaluation of λ_0 necessitates the solution of the above problem governing $\tilde{w}_0$.

8. Conformal mapping

With $\tilde{w}_0$ being harmonic, it may be embedded in a complex potential, say, ϕ,

$$\tilde{w}_0(\tilde{x}, \tilde{y}) = \text{Re}\{\phi(\tilde{z})\}, \tag{8.1}$$

wherein $\tilde{z} = \tilde{x} + i\tilde{y}$. We employ a conformal map, $\tilde{z} = g(\zeta)$, which transplants the upper-half complex ζ plane, where $\zeta = \xi + i\eta$, onto the fluid domain in the complex $\tilde{z}$ plane. Using the symmetry about the $\tilde{x}$ axis, we choose the critical points of the map in the manner specified in figure 5. With a slight abuse of notation, we denote the potential in the ζ plane as $\phi(\zeta)$ and its real part as $\tilde{w}_0(\xi, \eta)$. Since homogeneous Neumann and Dirichlet conditions are invariant under conformal maps (Brown & Churchill 2003), it follows that the shear-free condition becomes $\partial \tilde{w}_0 / \partial \eta = 0$ at $\eta = 0$ for $|\xi| > 1$, while the no-slip condition becomes $\tilde{w}_0 = 0$ at $\eta = 0$ for $|\xi| < 1$. Noting that condition (7.2) represents a net 'flux' of magnitude 2, it is transformed to a source at infinity, namely,

$$\phi \sim \frac{2}{\pi} \log \zeta \quad \text{as} \quad \zeta \to \infty \quad (\text{Im}\, \zeta > 0). \tag{8.2}$$

The problem governing $\tilde{w}_0$ is described in figure 5. We form an odd extension of it about the ξ axis, whereby the homogeneous Dirichlet condition there is trivially satisfied

and condition (8.2) gives

$$\tilde{w}_0 \sim \pm \frac{1}{\pi} \ln(\xi^2 + \eta^2) \quad \text{as} \quad \xi^2 + \eta^2 \to \infty \quad (\eta \gtrless 0). \tag{8.3}$$

The resulting problem is analogous to that governing the velocity potential of two-dimensional irrotational flow through an aperture (Milne-Thomson 1962), for which the solution is

$$\zeta = \cosh \frac{\pi \phi}{2}. \tag{8.4}$$

For the purpose of asymptotic matching, all we need is the local inversion of (8.4),

$$\phi \sim \frac{2}{\pi} \log(2\zeta) + \text{alg} \quad \text{as} \quad \text{Im}\, \zeta \to \infty, \tag{8.5}$$

wherein 'alg' denotes an algebraically small asymptotic error (smaller than some negative power of ζ). Approximation (8.5) constitutes the requisite refinement of (8.2) that is suitable for Van Dyke matching (Hinch 1991).

To proceed, we need the explicit form of the mapping. It is obtained using the Schwarz–Christoffel method (Brown & Churchill 2003) as

$$g(\zeta) = \frac{1}{2\pi}[\log(\zeta^2 - 1) - i\pi]. \tag{8.6}$$

Consistently with (8.5), there is no need for the full inversion of (8.6). Indeed, inverting at large $|\zeta|$ and substitution into (8.5) yields the refined version of (7.2):

$$\tilde{w}_0 \sim 2\tilde{x} + \frac{2}{\pi} \ln 2 \quad \text{as} \quad \tilde{x} \to \infty. \tag{8.7}$$

Plugging (6.5) and (8.7) into (7.3) yields the ord(1) slip length,

$$\lambda_0 = -\frac{10}{\pi} \ln 2. \tag{8.8}$$

9. Concluding remarks

Combining (5.4) with (8.8) yields the requisite two-term approximation,

$$\lambda \sim 2\epsilon^{-1} - \frac{10}{\pi} \ln 2 \quad \text{for} \quad \epsilon \ll 1, \tag{9.1}$$

where the asymptotic error is algebraically small. Formula (9.1) constitutes the key result of this paper. The predicted algebraic scaling is in sharp contrast with the logarithmic singularity observed for flat menisci in both the longitudinal (Crowdy 2021; Yariv 2023a) and transverse (Yariv 2023b) problems.

In the literature, large slipperiness of compound surfaces is typically associated with pillar arrays, where the slip length scales as $\epsilon^{-1/2}$ (Ybert *et al.* 2007; Davis & Lauga 2010; Schnitzer & Yariv 2018). This is also the scaling for 90°-protrusion-angle bubble mattresses in the conventional geometry, in the absence of groove invasion (Schnitzer 2016). The present slip-length prediction, scaling as ϵ^{-1}, suggests the possibility of enhanced slippage in grating configurations. It is interesting to note that partially invaded configurations are typically associated with curtailed slipperiness (Lee, Choi & Kim 2016); the present prediction thus illustrates yet another counter-intuitive feature of compound surfaces (Haase *et al.* 2016).

It is desirable to investigate the partially invaded geometry for protrusion angles different from $90°$, where a logarithmic singularity is expected. In the conventional geometry, that problem was solved by Schnitzer (2017). His solution explains the transition (at protrusion angles close to $90°$) from a logarithmic slip-length scaling to an algebraic one. The methodology is again one of matched asymptotic expansions, but the 'inner' region in the vicinity of the slat can no longer be handled using a lubrication approximation.

Declaration of interests. The author reports no conflict of interest.

Author ORCIDs.

Ehud Yariv https://orcid.org/0000-0003-0398-2954.

REFERENCES

BOCQUET, L. & BARRAT, J.-L. 2007 Flow boundary conditions from nano- to micro-scales. *Soft Matt.* **3** (6), 685–693.

BROWN, J.W. & CHURCHILL, R.V. 2003 *Complex Variables and Applications*. McGraw-Hill.

CHOI, C.-H. & KIM, C.-J. 2006 Large slip of aqueous liquid flow over a nanoengineered superhydrophobic surface. *Phys. Rev. Lett.* **96** (6), 066001.

CROWDY, D. 2010 Slip length for longitudinal shear flow over a dilute periodic mattress of protruding bubbles. *Phys. Fluids* **22** (12), 121703.

CROWDY, D. 2015 Effective slip lengths for longitudinal shear flow over partial-slip circular bubble mattresses. *Fluid Dyn. Res.* **47** (6), 1–14.

CROWDY, D.G. 2021 Slip length formulas for longitudinal shear flow over a superhydrophobic grating with partially filled cavities. *J. Fluid Mech.* **925**, R2.

DAVIS, A.M.J. & LAUGA, E. 2009 Geometric transition in friction for flow over a bubble mattress. *Phys. Fluids* **21** (1), 011701.

DAVIS, A.M.J. & LAUGA, E. 2010 Hydrodynamic friction of fakir-like superhydrophobic surfaces. *J. Fluid Mech.* **661**, 402–411.

HAASE, A.S., WOOD, J.A., LAMMERTINK, R.G.H. & SNOEIJER, J.H. 2016 Why bumpy is better: the role of the dissipation distribution in slip flow over a bubble mattress. *Phys. Rev. Fluids* **1** (5), 054101.

HINCH, E.J. 1991 *Perturbation Methods*. Cambridge University Press.

HOLMES, M.H. 2012 *Introduction to Perturbation Methods*. Texts in Applied Mathematics, vol. 20. Springer.

JOSEPH, P., COTTIN-BIZONNE, C., BENOÎT, J.-M., YBERT, C., JOURNET, C., TABELING, P. & BOCQUET, L. 2006 Slippage of water past superhydrophobic carbon nanotube forests in microchannels. *Phys. Rev. Lett.* **97** (15), 156104.

LAUGA, E. & STONE, H.A. 2003 Effective slip in pressure-driven Stokes flow. *J. Fluid Mech.* **489**, 55–77.

LEE, C., CHOI, C.-H. & KIM, C.-J. 2008 Structured surfaces for a giant liquid slip. *Phys. Rev. Lett.* **101** (6), 064501.

LEE, C., CHOI, C.-H. & KIM, C.-J. 2016 Superhydrophobic drag reduction in laminar flows: a critical review. *Exp. Fluids* **57** (12), 176.

LEE, C. & KIM, C.-J. 2009 Maximizing the giant liquid slip on superhydrophobic microstructures by nanostructuring their sidewalls. *Langmuir* **25** (21), 12812–12818.

LV, P., XUE, Y., SHI, Y., LIN, H. & DUAN, H. 2014 Metastable states and wetting transition of submerged superhydrophobic structures. *Phys. Rev. Lett.* **112** (19), 196101.

MILNE-THOMSON, L.M. 1962 *Theoretical Hydrodynamics*, 4th edn. Macmillan.

MIYOSHI, H., RODRIGUEZ-BROADBENT, H., CURRAN, A. & CROWDY, D. 2022 Longitudinal flow in superhydrophobic channels with partially invaded grooves. *J. Engng Maths* **137** (1), 3.

OU, J. & ROTHSTEIN, J.P. 2005 Direct velocity measurements of the flow past drag-reducing ultrahydrophobic surfaces. *Phys. Fluids* **17** (10), 103606.

PHILIP, J.R. 1972 Flows satisfying mixed no-slip and no-shear conditions. *Z. Angew. Math. Phys.* **23** (3), 353–372.

QUÉRÉ, D. 2005 Non-sticking drops. *Rep. Prog. Phys.* **68** (11), 2495–2532.

QUÉRÉ, D. 2008 Wetting and roughness. *Annu. Rev. Mater. Res.* **38** (1), 71–99.

ROTHSTEIN, J.P. 2010 Slip on superhydrophobic surfaces. *Annu. Rev. Fluid Mech.* **42** (1), 89–109.

SCHNITZER, O. 2016 Singular effective slip length for longitudinal flow over a dense bubble mattress. *Phys. Rev. Fluids* **1** (5), 052101(R).

SCHNITZER, O. 2017 Slip length for longitudinal shear flow over an arbitrary-protrusion-angle bubble mattress: the small-solid-fraction singularity. *J. Fluid Mech.* **820**, 580–603.

SCHNITZER, O. & YARIV, E. 2018 Small-solid-fraction approximations for the slip-length tensor of micropillared superhydrophobic surfaces. *J. Fluid Mech.* **843**, 637–652.

TSAI, P., PETERS, A.M., PIRAT, C., WESSLING, M., LAMMERTINK, R.G.H. & LOHSE, D. 2009 Quantifying effective slip length over micropatterned hydrophobic surfaces. *Phys. Fluids* **21** (11), 112002.

YARIV, E. 2023*a* Effective slip length for longitudinal shear flow over partially-invaded grooves: small solid-fraction approximations. *Phys. Rev. Fluids* **8**, L012101.

YARIV, E. 2023*b* Effective slip length for transverse shear flow over partially-invaded grooves. *J. Fluid Mech.* **957**, R1.

YARIV, E. & SCHNITZER, O. 2018 Pressure-driven plug flows between superhydrophobic surfaces of closely spaced circular bubbles. *J. Engng Maths* **111**, 15–22.

YBERT, C., BARENTIN, C., COTTIN-BIZONNE, C., JOSEPH, P. & BOCQUET, L. 2007 Achieving large slip with superhydrophobic surfaces: scaling laws for generic geometries. *Phys. Fluids* **19** (12), 123601.